Extended Abstracts of the 1993 International Conference on Solid State Devices and Materials, Makuhari, 1993, pp. 624-626

Electron Tunneling Through Ultra-Thin Gate Oxide Formed on Hydrogen-Terminated Si(100) Surfaces

M. Hiroshima, T. Yasaka, S. Miyazaki and M. Hirose

Department of Electrical Engineering, Hiroshima University

Higashi-Hiroshima 724, Japan

Current transport through ultra-thin gate oxide grown on Si(100) surfaces has been systematically investigated. It is shown that the current through oxides thinner than 4.2 nm is controlled by the direct tunneling (DT), while Fowler Nordheim tunneling (FNT) predominates the transport through SiO_2 thicker than 5.1 nm. The oxide thickness range between 4.2 and 5.1 nm DT limits the current at low electric fields and FNT at high fields. The observed tunneling current is quantitatively explained by the theory based on the WKB approximation. Also, the influence of the Si surface microroughness on the tunneling current is discussed.

1. INTRODUCTION

ULSI devices beyond 0.14 μm feature size need reliable gate oxides thinner than 5 nm. For better control of the oxide quality, it is necessary to quantitatively understand the tunneling mechanism and to model the transport. In addition, the atomic-scale microroughness of Si(100) surfaces are thought to be correlated with the SiO_2/Si interface structure because the silicon oxidation proceeds through a layer-by-layer mechanism[1~3]. This raises a question as to whether or not the surface microroughness influences the electron tunneling process. FT-IR-ATR(Attenuated Total Reflection)[4] or AFM (Atomic Force Microscope)[3,5] is generally used to characterize the flatness of Si wafer surfaces. It is already shown by AFM that SC-1 clean in NH_4OH:H_2O_2:H_2O=1:1:5 makes a Si(100) surface rough and the reduction of NH_4OH content to 0.8% is effective to improve the surface morphology[5,6]. The atomic scale surface morphology is in principle obtained by AFM, although the radius of the probe head limits the resolution and experimental artifacts must be carefully minimized, while ATR obviously detects the hydrogen bonding features of a dilute HF-treated surface and reveals the atomic scale microroughness. In this paper, the tunneling current transport through ultra-thin gate oxides on Si(100) surfaces has been quantitatively evaluated by comparing the observed current with the one computed on the basis of the WKB approximation. Influence of the surface morphology on the tunneling characteristics is also discussed in connection with the results of AFM and ATR.

2. EXPERIMENTAL

The Si wafers were precleaned in a boiling solution of HCl:H_2O_2:H_2O=3:11:86 and subsequently dipped in NH_4OH:H_2O_2:H_2O=3:3:7 for 2 min at room temperature and finally in 4.5%HF. Thus treated Si(100) surfaces are terminated with hydrogen and hardly oxidized in clean room air for up to 20 minutes[7]. Further the wafers were cleaned in NH_4OH:H_2O_2:H_2O=0.15:3:7 at 85°C for 10 min and treated in 0.1% HF + 1% H_2O_2 in order to obtain flatter (100) surfaces. For fabricating tunnel MOS structures, the thermal oxidation was carried out at 1000°C in 2% dry O_2 diluted with N_2. Al gate electrodes with a diameter of 1 mm were evaporated through a mask.

3. RESULTS AND DISCUSSION

It is known that an atomically-flat Si(111) surface can be obtained by cleaning the wafer in a BHF solution with pH=5.3 or higher as demonstrated by ATR[4]. In contrast to this, the Si(100) surface cleaned in HCl:H_2O_2:H_2O=3:11:86 and subsequently dipped in NH_4OH:H_2O_2:H_2O=3:3:7 could not be planarized by BHF(pH=5.3) as clearly shown by ATR spectrum in Fig. 1 a, where the SiH_2 symmetric vibrational peak appears together with a strong SiH_3 absorption peak. The result is almost the same for the case of 4.5% or 0.1%HF treatment although the asymmetric SiH_2 band is predominant (Fig.1 b and c). In the Si(100) wafer cleaning by an NH_4OH:H_2O_2:H_2O solution, it is recommended to lower the NH_4OH content[5,6]. Nevertheless, NH_4OH:H_2O_2:H_2O=0.15:3:7 clean followed by 4.5% HF treatment provide a spectrum very similar to Fig. 1 b as indicated in Fig. 2 (a). In order to get a flatter Si(100) surface, it is assumed that the reactive sites such as atomic steps or microfacets existing on the terrace surface should be selectively oxidized by oxygen supplied from H_2O_2 and subsequent removal of the oxide should be performed by dilute HF. Hence, the wafer is precleaned in boiling solution of NH_4OH:H_2O_2:H_2O=0.15:3:7 and dipped in 4.5%HF and in a 0.1%HF+1%H_2O_2 solution. A sharp SiH_2 peak accompanied with weak SiH and SiH_3 absorption bands is obtained (Fig. 2 (b)), and the surface is flatter than the case of Fig. 1 and Fig. 2 (a). The extent of the surface microroughness for the samples shown in Fig. 2 is also probed by AFM as illustrated in Fig. 3. The images provide an average microroughness Ra=0.18 nm for the case of Fig. 3 (a) and Ra=0.19 nm for Fig. 3 (b).

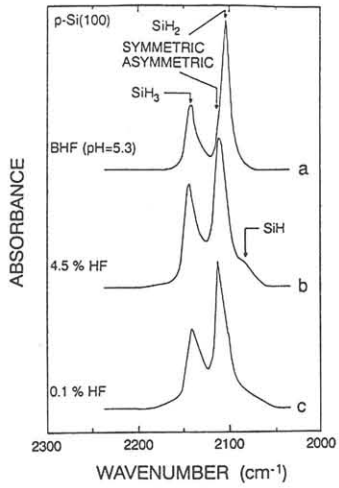

Fig. 1 SiH_x stretching absorption spectra of p-Si(100) surfaces treated in BHF (pH = 5.3), 4.5% HF (pH=1.0~1.2), or 0.1% HF (pH = 1.9). The spectra are normalized with the SiH_2 peak intensity. The preclean was made in $NH_4OH:H_2O_2:H_2O$ =3:3:7 for 2 min at room temperature.

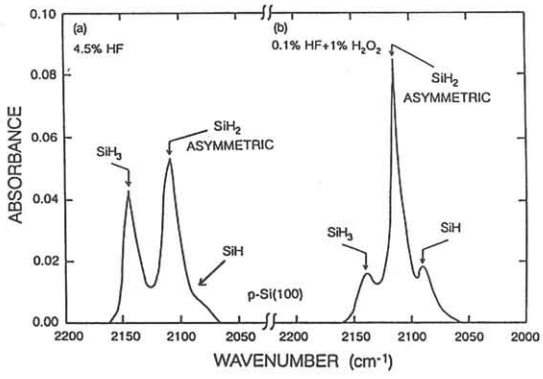

Fig. 2 ATR spectra of p-Si(100) surfaces. The wafers were cleaned in $NH_4OH:H_2O_2:H_2O$ =0.15:3:7 at 85 °C and subsequently dipped in 4.5 % HF (a). Further treatment was made in 0.1% HF + 1% H_2O_2 (b).

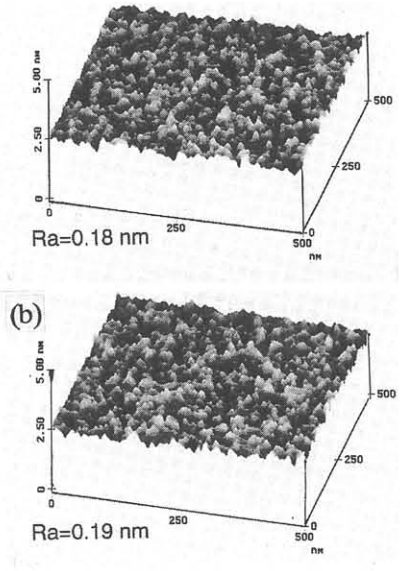

Fig. 3 AFM images of p-Si(100) surfaces. The wafers were cleaned in $NH_4OH:H_2O_2:H_2O$ =0.15:3:7 at 85 °C and subsequently dipped in 4.5 % HF (a). Further treatment was made in 0.1% HF + 1% H_2O_2 (b).

The different surface morphology as revealed by ATR can not be discriminated by AFM. As far as the AFM images are concerned, the surface is flat enough with respect to the single atom step height of 0.136 nm on the Si(100) surface. Therefore, these comparable Ra values indicate that AFM with a probe radius of 35~40 nm is not sensitive enough to detect significantly different atomic-scale morphology of the surfaces identified by ATR spectra because the horizontal resolution of the present AFM is 8.3~8.9 nm. It is possible that the Si surface morphology before the oxidation influences the SiO_2/Si interface morphology. Hence, we have compared the tunneling current through ultra-thin SiO_2 grown on Si with different surface microroughnesses. Tunneling current versus oxide voltage characteristics are compared in Fig. 4 for wafers treated in different chemical solutions. Wafers were cleaned in a solution of $NH_4OH:H_2O_2:H_2O$=3:3:7 for 2 min at room temperature and subsequently in 4.5% HF (case A) or they were treated in 0.1%HF+1%H_2O_2 after the $NH_4OH:H_2O_2:H_2O$=0.15:3:7 clean (case B). As is clearly shown in the figure, the tunneling current decreases with an increase of oxide thickness. The current density is quantitatively evaluated by using the following equations:
For direct tunneling,

$$J = \frac{q^2(\phi_B - V_{ox}/2)}{2\pi h t_{ox}^2} \exp\left[-4\pi t_{ox}(2qm^*)^{\frac{1}{2}} \times (\phi_B - V_{ox}/2)^{\frac{1}{2}}/h\right], \quad (1)$$

and for Fowler-Nordheim tunneling[8],

$$J = \frac{q^3 E_{ox}^2}{8\pi h \phi_B} \exp\left[-8\pi(2m^*)^{\frac{1}{2}} \phi_B^{3/2}/3hqE_{ox}\right]. \quad (2)$$

Here, q is the electronic charge, t_{ox} the oxide thickness, h the Planck constant, V_{ox} the voltage across the oxide, $E_{ox}=V_{ox}/t_{ox}$, ϕ_B the barrier height at the Al/SiO_2 interface and m^* the tunneling electron effective mass. The theoretical I-V curves are computed and compared with the result of Fig. 4. The tunneling electron effective mass is the only parameter to fit the calculated current to the measured one. The barrier height at the Al/SiO_2 interface ϕ_B = 3.17eV is employed. The I-V curves for samples (B) as denoted by curves ②, ④ and ⑦ in Fig. 4 are compared with the calculated result as shown in

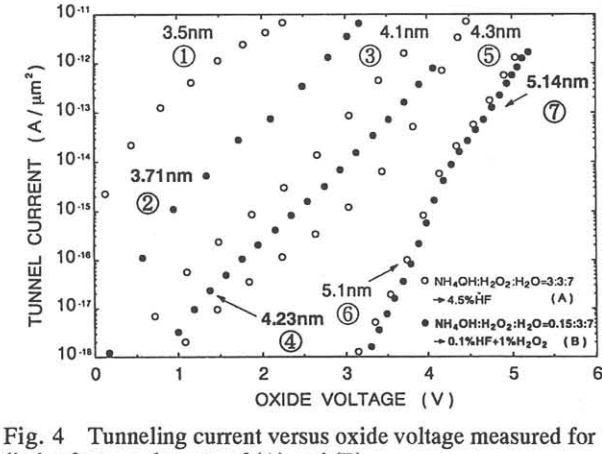

Fig. 4 Tunneling current versus oxide voltage measured for MOS diodes for samples sets of (A) and (B).

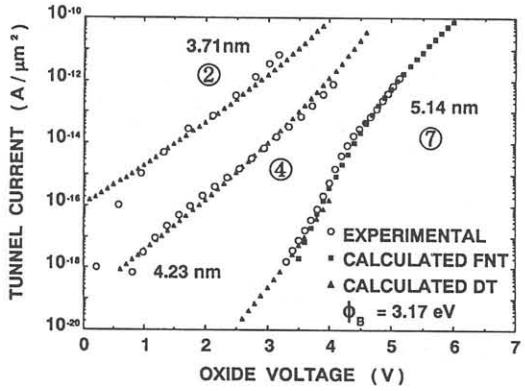

Fig. 5 Tunneling current versus oxide voltage characteristics measured for MOS (samples (B)) with different oxide thicknesses are compared with the calculated result.

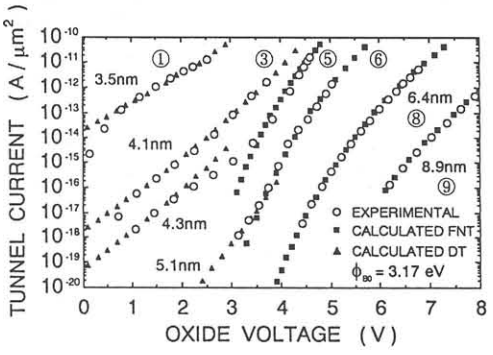

Fig. 6 Tunneling current versus oxide voltage measured for MOS diodes for samples (A), ⑧ and ⑨ with different oxide thicknesses are compared with the calculated characteristics.

Fig. 5. Also, the tunneling current for samples (A) such as curves ①, ③ and ⑥ is also fitted to eqs. (1) and (2) as indicated in Fig. 6. The electron effective mass thus obtained as a fitting parameter is shown in Fig. 7, where the effective mass for the direct tunneling (DT) is 0.32 m_0 for both sets of samples (A) and (B). Curves ⑤, ⑥, ⑦, ⑧ and ⑨ in Figs. 5 and 6 provide the other effective mass corresponding to Fowler-Nordheim tunneling (see Fig.7). The effective mass difference for the case of DT and FNT could be explained by the fact that DT occurs from the Al gate to the Si conduction band while FNT from the Fermi level of the Al gate to the SiO_2 conduction band and that the electron effective mass in SiO_2 is larger than that in Si. It is shown from Figs. 5 and 6 that the current transport through SiO_2 thicker than 5.1nm is controlled by FNT while DT dominates the current through SiO_2 thinner than 4.2 nm. In the oxide thickness range 4.3 to 5.1 nm the FNT mechanism controls the current at the oxide voltages above 3.5V, and DT limits the current below 3.0V. Note that the tunneling current through 4.3 nm thick SiO_2 in Fig. 6 obviously shows the change in the current transport mechanism from DT to FNT in the oxide voltage range 3 to 3.5V where the onset of triangular barrier formation occurs and FNT mechanism becomes more important. This result is also consistent with the previously measured Al/SiO_2 barrier height ϕ_B = 3.17eV[9].

The electron tunneling mechanism in SiO_2 is clarified by noting the oxide thickness and the oxide electric field strength as illustrated in Fig. 8, where the solid curve refers to the theoretically predicted boundary at which the predominant transport mechanism is changed. The solid curve is obtained by equating the calculated FNT current density to the calculated DT current density.

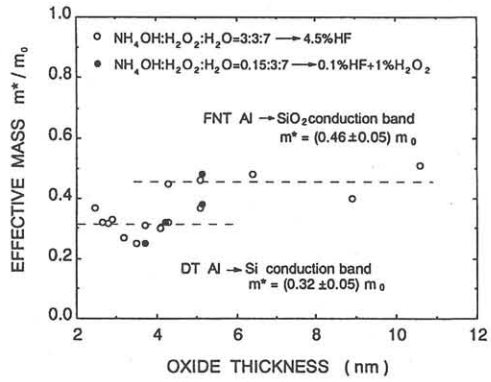

Fig. 7 Tunneling effective mass obtained as a fitting parameter for I-V curves in Figs. 5 and 6 as a function of oxide thickness.

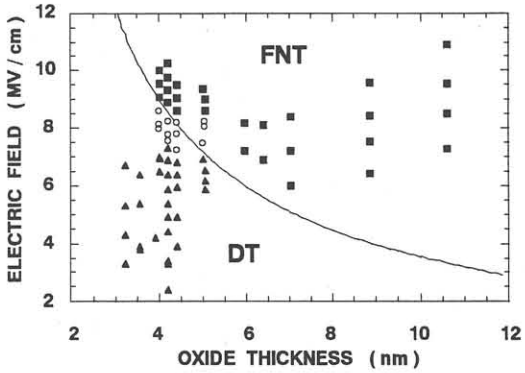

Fig. 8 Current transport mechanism discriminated by oxide thickness and oxide electric field strength. The solid curve is theoretically predicted boundary between FNT and DT. Mark ■ refers to FNT, ▲ to DT and ○ to the transition region from DT mechanism to FNT.

In conclusion, nearly ideal tunneling transport is confirmed for ultra-thin SiO_2 grown on well-defined hydrogen-terminated Si (100) surfaces. The difference in Si surface morphology as characterized by ATR is not directly correlated with the tunneling current.

REFERENCES

1) M. Morita, T. Ohmi, E. Hasegawa, M. Kawakami and K. Suma, Appl. Phys. Lett. 55(1989) 562.
2) T. Yasaka, M. Takakura, S. Miyazaki and M. Hirose, Mat. Res. Soc. Symp. Proc. 222(1991) 225.
3) Y. Homma, M. Suzuki and N. Yabumoto, J. Vac. Sci. Technol. 10(1992) 2055.
4) G. S. Higashi, Y. J. Chabal, G. W. Trucks and K. Raghavachari, Appl. Phys. Lett. 56(1990) 656.
5) T. Ohmi, M. Miyashita, M. Itano, T. Imaoka and I. Kawanabe, IEEE Trans. Electron Devices 39(1992) 573.
6) M. M. Heyns, M. Meuris, S. Verhaverbeke, P. W. Mertens, A. Philipossian, D. Gräf and A. Schnegg, Extended Abstract of 24th Conference on SSDM, Tsukuba, 1992, p. 187.
7) T. Sunada, T. Yasaka, M. Takakura, S. Miyazaki and M. Hirose, Jpn. J. Appl. Phys. 29(1990) 2408 .
8) M. Lenzlinger and E. H. Snow, J. Appl. Phys. 40(1969) 278.
9) J. Maserjian, Physics and Chemistry of SiO_2 and the Si-SiO_2 Interface, eds. C. R. Helms and B. E Deal (Plenum Press, NY, 1989) pp. 497.